

# UCSF

## UC San Francisco Previously Published Works

### Title

A Systematic Approach to the Discovery of Protein-Protein Interaction Stabilizers

### Permalink

<https://escholarship.org/uc/item/3wf7v84h>

### Journal

ACS Central Science, 9(5)

### ISSN

2374-7943

### Authors

Kenanova, Dyana N  
Visser, Emira J  
Virta, Johanna M  
[et al.](#)

### Publication Date

2023-05-24

### DOI

10.1021/acscentsci.2c01449

Peer reviewed

# A Systematic Approach to the Discovery of Protein–Protein Interaction Stabilizers

Dyana N. Kenanova,<sup>⊥</sup> Emira J. Visser,<sup>⊥</sup> Johanna M. Virta, Eline Sijbesma, Federica Centorrino, Holly R. Vickery, Mengqi Zhong, R. Jeffrey Neitz, Luc Brunsveld,\* Christian Ottmann,\* and Michelle R. Arkin\*



Cite This: *ACS Cent. Sci.* 2023, 9, 937–946



Read Online

ACCESS |



Metrics & More

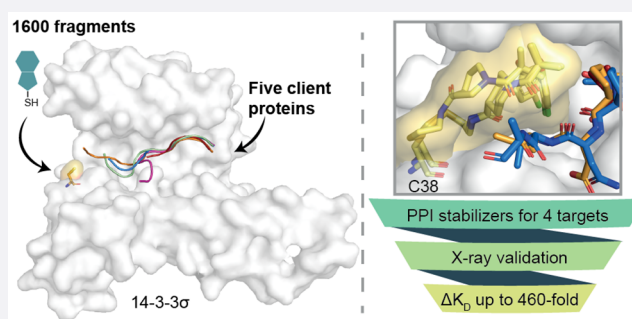


Article Recommendations



Supporting Information

**ABSTRACT:** Dysregulation of protein–protein interactions (PPIs) commonly leads to disease. PPI stabilization has only recently been systematically explored for drug discovery despite being a powerful approach to selectively target intrinsically disordered proteins and hub proteins, like 14-3-3, with multiple interaction partners. Disulfide tethering is a site-directed fragment-based drug discovery (FBDD) methodology for identifying reversibly covalent small molecules. We explored the scope of disulfide tethering for the discovery of selective PPI stabilizers (molecular glues) using the hub protein 14-3-3 $\sigma$ . We screened complexes of 14-3-3 with 5 biologically and structurally diverse phosphopeptides derived from the 14-3-3 client proteins ER $\alpha$ , FOXO1, C-RAF, USP8, and SOS1. Stabilizing fragments were found for 4/5 client complexes. Structural elucidation of these complexes revealed the ability of some peptides to conformationally adapt to make productive interactions with the tethered fragments. We validated eight fragment stabilizers, six of which showed selectivity for one phosphopeptide client, and structurally characterized two nonselective hits and four fragments that selectively stabilized C-RAF or FOXO1. The most efficacious fragment increased 14-3-3 $\sigma$ /C-RAF phosphopeptide affinity by 430-fold. Disulfide tethering to the wildtype C38 in 14-3-3 $\sigma$  provided diverse structures for future optimization of 14-3-3/client stabilizers and highlighted a systematic method to discover molecular glues.



## INTRODUCTION

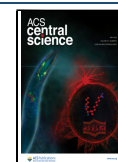
Protein–protein interactions (PPIs) are essential to biology, and their dysregulation is central to many diseases including cancer and neurodegeneration.<sup>1–4</sup> Many of these important PPIs include “hub proteins” that interact with a large number of protein partners, ranging from a few dozen to a few thousand.<sup>5</sup> Small molecules that inhibit or stabilize individual PPIs within these networks would be powerful tools to understand the effect of a single PPI on cellular function. Although PPIs were historically considered “undruggable”, there has been much progress in developing small molecule PPI inhibitors as biological probes and therapeutics.<sup>6–10</sup> By contrast, PPI stabilization has remained largely underexplored, despite its potential to be a selective method for the manipulation of a single interaction within a protein network.<sup>11,12</sup> Stabilization also has the potential to target unstructured, difficult to drug proteins via composite PPI binding pockets.<sup>13,14</sup> Molecular glue degraders and natural products have demonstrated the therapeutic value of stabilizing native or non-native (neomorphic) PPIs.<sup>15–17</sup> However, there are few robust, generalizable strategies to discover PPI stabilizers prospectively.<sup>11,18</sup> Here, we describe a robust and

instructive approach, using site-directed fragment based drug discovery (FBDD) to systematically discover molecular glues.

FBDD is a well-established method for the discovery of small molecules toward challenging targets.<sup>19,20</sup> Fragments are simple chemical building blocks that—owing to their small number of atoms—sample chemical space efficiently. FBDD involves screening for weakly binding fragments that target subsites within a binding site, followed by fragment optimization via linking two fragments or elaborating a fragment-sized core. Disulfide tethering is a method of FBDD that capitalizes on a native or engineered cysteine residue proximal to an envisaged ligand binding site.<sup>21–24</sup> In the context of orthosteric PPI stabilization, this binding site is composed of both members of the protein complex (the composite PPI interface). Fragments that bind to this site with the correct positioning to form a protein–fragment disulfide

Received: December 5, 2022

Published: April 18, 2023



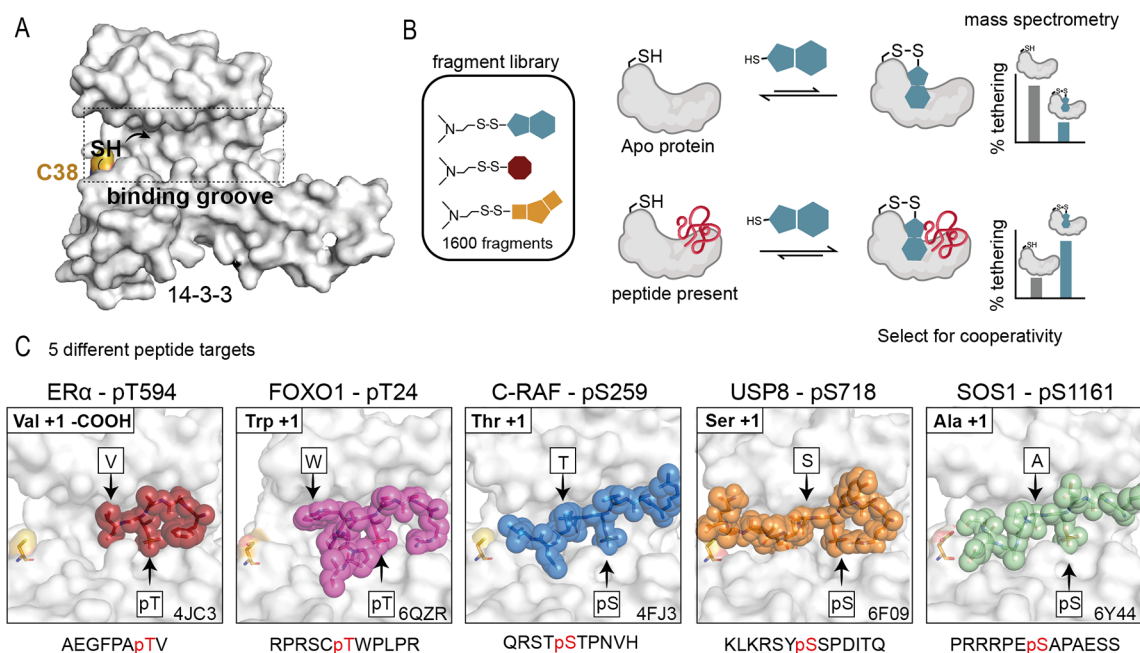


**Figure 1.** 14-3-3/client stabilizer approach. (A) The client protein binding groove of a 14-3-3 $\sigma$  monomer (white surface) highlighting the native cysteine (C38; yellow surface) and target thiol. (B) General schematic of the primary disulfide tethering screen. Fragments were incubated with *apo* 14-3-3 $\sigma$  (white) without any phosphopeptide (top) and 14-3-3 $\sigma$  with the phosphopeptide client present (bottom). Fragments were assessed for their covalent engagement of C38 via mass spectrometry, termed “% tethering”. Fragments that bound 14-3-3 $\sigma$  with a higher % tethering in the presence of phosphopeptide than in the *apo* screen were selected for further analysis of cooperativity. (C) Crystallographic structures of the 5 phosphopeptide clients bound in the 14-3-3 $\sigma$  (white surface) binding pocket showing proximity to C38 (yellow surface). ER $\alpha$  (red sticks) has a C-terminal motif with phosphothreonine (pT) in the penultimate position and C-terminal valine (V) in the +1 position. FOXO1 (pink sticks) has a curved motif with tryptophan (W) in the +1 position. C-RAF (blue sticks), USP8 (orange sticks), and SOS1 (green sticks) extend to various degrees into the 14-3-3 binding groove, with threonine (T), serine (S), and alanine (A) residues in the +1 position, respectively. PDB left to right: 4JC3, 6QZR, 4FJ3, 6F09, 6Y44.

bond are detected by intact protein mass spectrometry (MS) in a high-throughput screen.<sup>25</sup> We utilize a library of approximately 1600 disulfide molecules with diverse fragments and linkers between the fragment and the disulfide.<sup>26</sup> To test the efficacy of this technology to discover PPI stabilizers, we have selected the hub protein 14-3-3 and a set of its diverse partner proteins.

14-3-3 is ubiquitously expressed in mammals and plays multiple roles within the cell, including phosphorylation protection, conformational changes, subcellular trafficking, and induction or disruption of other PPIs.<sup>13,27–29</sup> 14-3-3 typically binds to a phosphorylated serine/threonine in intrinsically disordered regions of its clients.<sup>30</sup> With several hundred known interacting partners, the 14-3-3-binding proteome provides diverse PPI interfaces with which to test the scope and limitations of our screening technology. Furthermore, 14-3-3/client stabilization could lead to therapeutics in a variety of disease fields including oncology, neurodegeneration, inflammation, and metabolic disease.<sup>29,31</sup> Previous studies using natural products such as fusicoccin (FC-A) and cotylenin-A (CN-A) have shown that stabilizing 14-3-3/client interactions regulates the activity of important cell signaling pathways including estrogen receptor  $\alpha$  (ER $\alpha$ ) and C-RAF, respectively.<sup>14,32</sup>

We recently demonstrated the utility of disulfide tethering to identify molecular glues of the 14-3-3/ER $\alpha$  PPI. We discovered a series of disulfide fragments that stabilized the complex when bound to an engineered cysteine residue in the binding groove of 14-3-3, enhancing binding of the ER $\alpha$  C-

terminal phosphopeptide up to 40-fold.<sup>25</sup> We now focus on targeting the native cysteine found in the 14-3-3 sigma isoform (14-3-3 $\sigma$ ), which offers greater translatability for covalent molecules. Of the 7 isoforms found in mammalian cells, 14-3-3 $\sigma$  is the only one that harbors a cysteine residue proximal to the client binding groove, providing an additional degree of isoform specificity (Figure 1A).<sup>30</sup> The Protein Data Bank contains dozens of crystallographic structures of 14-3-3 with bound phosphopeptides derived from many of its binding partners, as well as a few examples of CryoEM structures of full length proteins.<sup>13,33–35</sup> This wealth of structural information allows for direct visualization of the various 14-3-3/client binding interfaces which could be capitalized on for the discovery of selective fragment stabilizers and the development of potent lead compounds through structure-guided chemical optimization. For our screens, we utilized the phosphopeptide mimetics of 14-3-3 PPI partners which bind 14-3-3 in a similar fashion to the unstructured regions of the full-length proteins but offer greater synthetic flexibility and simplified crystallography.<sup>13,34</sup>

Here, we used the disulfide tethering technology to systematically achieve selective PPI stabilization of 14-3-3 client phosphopeptides with diverse sequences and structures. The selected clients are also modulated by 14-3-3 in a way that could be therapeutically useful in cancer, metabolic disease, and/or rare disease.<sup>14,36–39</sup> For four of the five targets, effective PPI stabilizers were identified. Crystallographic and functional data highlight the molecular recognition of fragments for the distinctive composite PPI interfaces formed by 14-3-3 bound

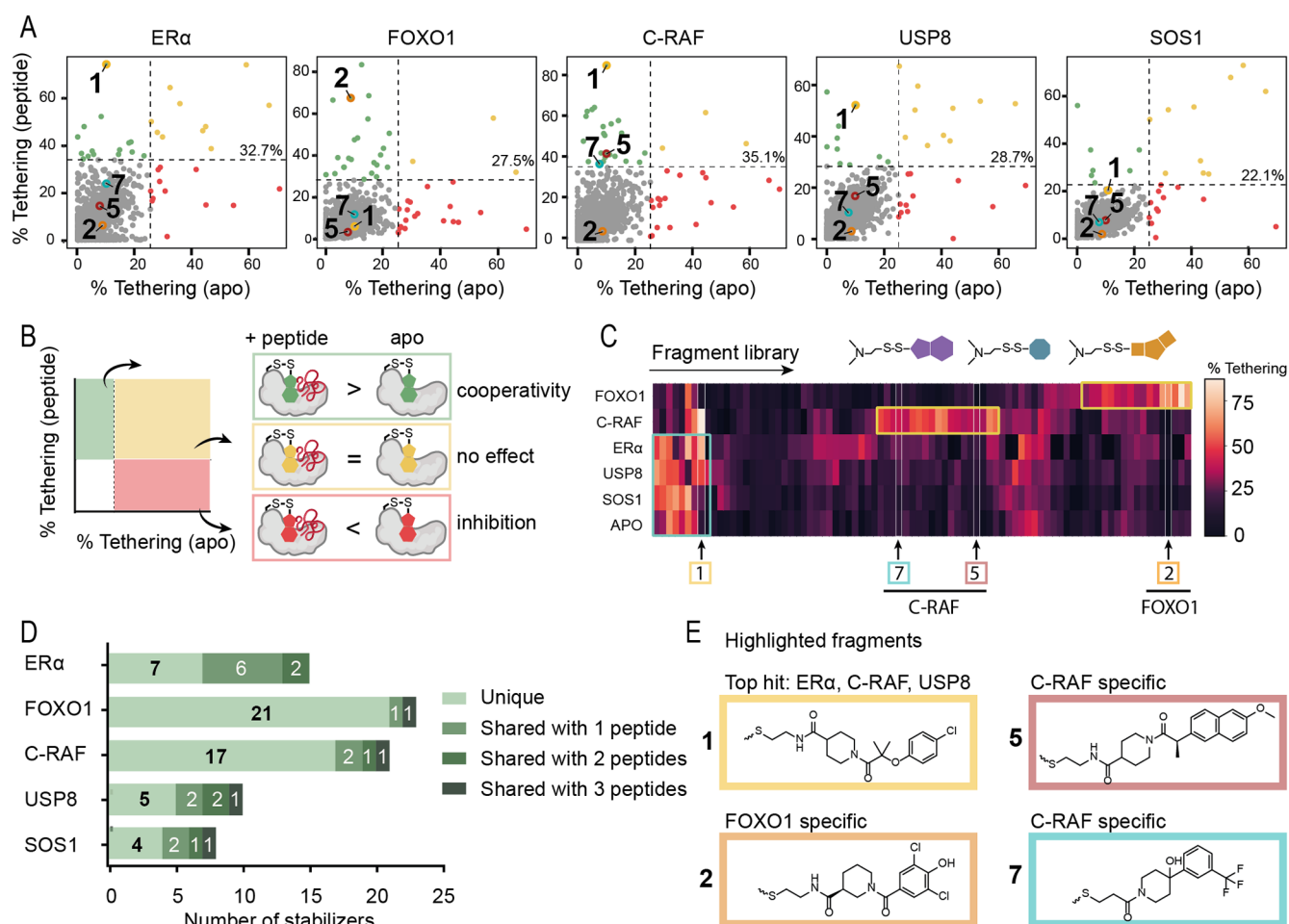


**Figure 2.** Primary tethering screen results. (A) Scatterplot data illustrating the correlation of % tethering of fragments to 14-3-3 $\sigma$  in the presence of the phosphopeptide (*y*-axis) as compared to *apo* 14-3-3 $\sigma$  (*x*-axis). Hit selection threshold (mean + 3\*SD) in each screen is indicated by a black dashed line. Compounds 1, 2, 5, and 7 are indicated as yellow, orange, red, and cyan circles, respectively. (B) Schematic of compound scatterplots. Quadrants are outlined by dotted lines signifying 3\*SD above average % tethering for compounds in the presence of phosphopeptide (horizontal line) and *apo* 14-3-3 $\sigma$  (vertical line). Compounds in the green quadrant showed increased binding to 14-3-3 $\sigma$  in the presence of phosphopeptide, the yellow quadrant showed neutral binding to 14-3-3 $\sigma$ , and the red quadrant showed a reduced binding in the presence of phosphopeptide. (C) Heat map of hit fragments across all 5 phosphopeptide screens and *apo* 14-3-3 $\sigma$  screen. Compounds clustered based on % tethering in each screen. Compounds 1, 2, 5, and 7 were of primary interest as nonselective and selective stabilizers. (D) Number of stabilizers of each peptide that were unique, shared with one other peptide, shared with two other peptides, or shared with three other peptides (green bars with the darker color shared with more peptides). (E) Chemical structures of highlighted fragment hits 1, 2, 5, and 7.

to client phosphopeptides. In particular, the C-RAF- and FOXO1-based peptide–protein interactions with 14-3-3 yielded fragments with high selectivity and/or stabilization factors. The diversity of sequences and conformations found in 14-3-3/client complexes makes the 14-3-3 interactome particularly promising for small-molecule PPI stabilization; furthermore, the disulfide tethering approach is remarkably effective at selecting chemical starting points for further design of potent and selective PPI stabilizers.

## RESULTS AND DISCUSSION

**Primary Screen for 14-3-3/Client Stabilizers.** The disulfide tethering screen targeted C38, a native cysteine on 14-3-3 $\sigma$  located proximal to the natural product binding pocket within the phosphopeptide recognition groove (Figure 1A, Figure S1). The cysteine forms a reversible covalent bond with the fragment thiol through disulfide exchange; the amount of bound fragment is measured by MS. A fragment stabilizer is expected to show a higher “% tethering” in the presence of the

14-3-3 $\sigma$ /client phosphopeptide complex than 14-3-3 $\sigma$  alone due to cooperativity between the fragment and the peptide (Figure 1B). The screening was performed on five different peptide targets displaying three conceptually distinct 14-3-3 interaction motifs (Figure 1C): truncated (ER $\alpha$ ),<sup>14,40</sup> turned (FOXO1),<sup>37</sup> and linear (C-RAF, USP8, SOS1).<sup>32,35,38,41</sup>

14-3-3 $\sigma$  (100 nM) was screened in complex with the 5 client phosphopeptides at a concentration twice their respective  $K_D$  values (Figure S2). This condition provided a consistent presence of the 14-3-3 $\sigma$ /phosphopeptide composite interface that the fragments would engage. The 14-3-3 $\sigma$ /phosphopeptide complex was incubated with a single concentration of fragment (200  $\mu$ M) under reducing conditions (250  $\mu$ M  $\beta$ -mercaptoethanol) for 3 h before samples were measured by intact-protein LC/MS. The % tethering threshold for hit selection was three standard deviations (3\*SD) above the average % tethering for that condition (Figure 2A). In the quadrant of highest interest, potential stabilizing fragments showed % tethering above the tethering threshold in the

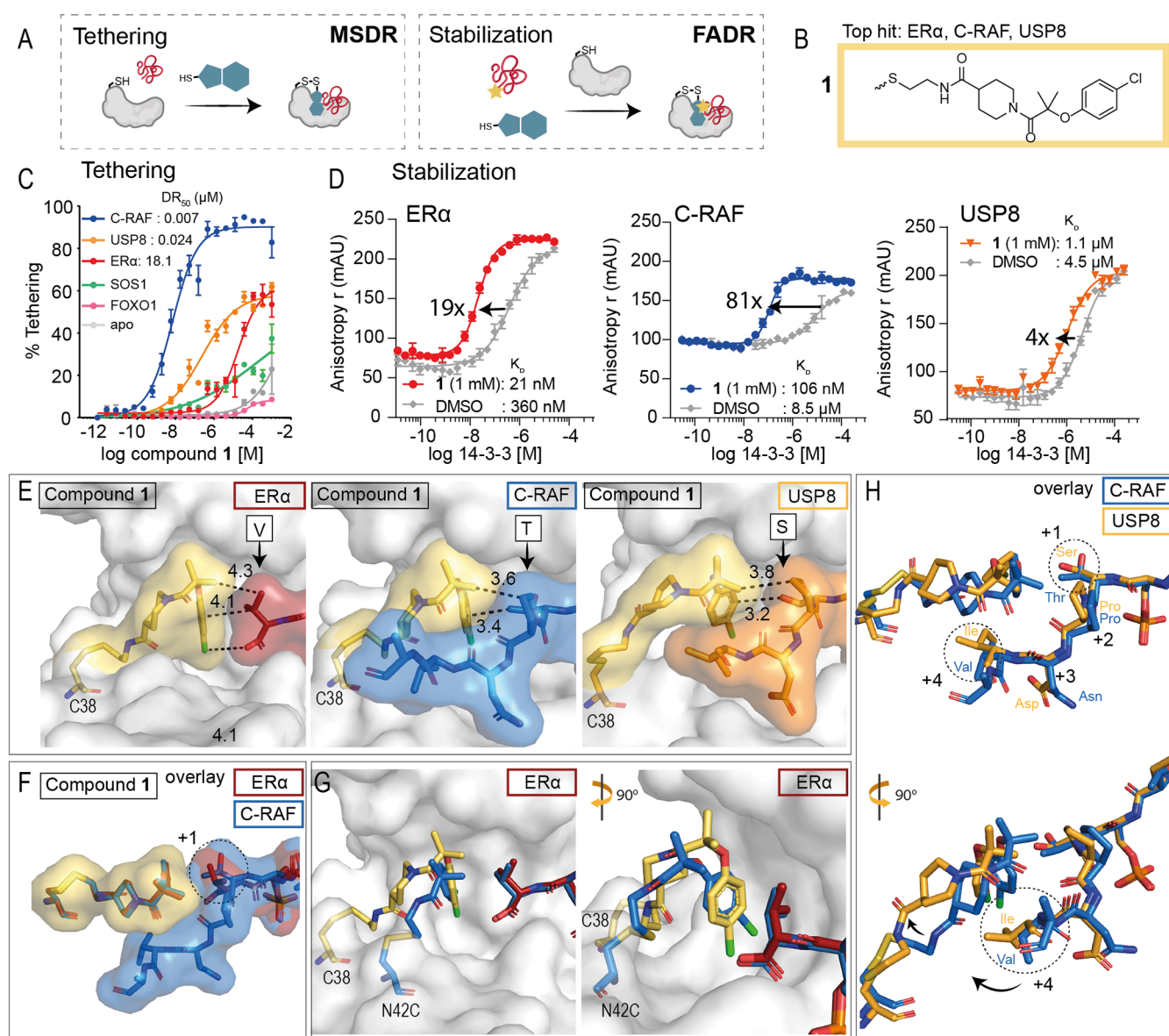


**Figure 3.** Overview of biochemical and structural properties of nonselective stabilizer **1**. (A) In MS dose response (MSDR), the focus was on compound binding to 14-3-3σ, measured by % tethering; fluorescence anisotropy dose response (FADR) experiments determined the degree of stabilization, measured by phosphopeptide binding to 14-3-3σ in the presence of compound. (B) Chemical structure of stabilizer **1**. (C) MSDR curves for **1** showing percentage of fragment/protein conjugate formation with 14-3-3σ *apo*, or in the presence of ERα, FOXO1, C-RAF, USP8, or SOS1 peptide. (D) 14-3-3σ titrations to fluorescein-labeled ERα, C-RAF, or USP8 in the presence of DMSO or **1** (1 mM), reporting a 19-, 81-, and 4-fold increase of the 14-3-3σ/peptide binding interface, respectively. (E) Crystal structure of **1** bound to 14-3-3σ C38 in complex with (from left to right) ERα peptide, C-RAF peptide, and USP8 peptide. Distances are indicated (Å, black dashes). (F) Overlay of **1**'s conformations when interacting with ERα and C-RAF. (G) Overlay of **1** (yellow) bound to 14-3-3σ C38 and previously reported stabilizer (blue) bound to 14-3-3σ mutant N42C (PDB ID: 6HMT) interacting with ERα phosphopeptides. (H) Overlay of **1** bound to 14-3-3σ C38 interacting with C-RAF and USP8.

peptide screen and % tethering below the tethering threshold in the *apo* screen (Figure 2B, green quadrant). Neutral compounds showed significant % tethering for both 14-3-3σ/phosphopeptide and *apo* (Figure 2B, yellow quadrant). Potential inhibitory fragments showed significant % tethering above the tethering threshold in the *apo* screen but not in the presence of peptide (Figures 2B, red quadrant). Compounds were clustered in a heat map based on % tethering in each of the five peptide screens and *apo* 14-3-3 screen (Figure 2C). An overlapping fragment hit cluster was identified for ERα, USP8, and SOS1 (Figure 2C, green box), whereas a cluster of unique

hit fragments was identified for both C-RAF and FOXO1 (Figure 2C, yellow boxes), indicating a difference in the abundance of selective stabilizers from the primary screens.

Each 14-3-3σ/phosphopeptide screen yielded potential stabilizing fragments, but the number and binding efficiency varied (Figure 2A,C,D, and Tables S1–S5). The initial screen for ERα yielded 15 hit fragments including 7 unique stabilizers and a 33% tethering threshold. The FOXO1 screen yielded 23 hit fragments including 21 unique stabilizers and a 28% tethering threshold. The C-RAF screen yielded 21 fragments including 16 unique stabilizers and a 35% tethering threshold.

The USP8 screen yielded 10 hit fragments including 5 unique stabilizers and a 29% tethering threshold. The SOS1 screen yielded 8 hit fragments including 4 unique stabilizers and a 22% tethering threshold (Figure 2A,D). Figure 2E depicts representative chemical structures for each target.

**Nonselective Stabilizing Compound 1.** In the initial screen, compound **1** was identified as top hit for ER $\alpha$ , C-RAF, and USP8 (Figure 2). **1** was further characterized by three dose–response experiments. Mass spectrometry (MSDR, analyzing fragment binding to protein, quantified by DR<sub>50</sub> values) and fluorescent anisotropy (FADR, analyzing peptide binding to protein in the presence of compound, quantified by EC<sub>50</sub> values) defined the binding affinity for the fragment and its effective concentration, respectively (Figure 3A). The compound's effect on the 14-3-3/client PPI was then determined by titrating 14-3-3 in a fluorescence anisotropy assay at constant peptide and compound concentrations (quantified by K<sub>D\_app</sub>). In all three validation assays, **1** displayed a strong preference for C-RAF, followed by ER $\alpha$  and USP8, and had no activity with FOXO1 or SOS1. Compound **1** showed DR<sub>50</sub> values of 7 nM for C-RAF, 18.1  $\mu$ M for ER $\alpha$ , and 24 nM for USP8 (Figure 3C) as well as EC<sub>50</sub> values of 922 nM for C-RAF, 1.31  $\mu$ M for ER $\alpha$ , and 3.38  $\mu$ M for USP8 (Figure S3). In the protein titrations, **1** increased peptide affinity for 14-3-3 $\sigma$  by 81-fold in the C-RAF complex, 19-fold for 14-3-3 $\sigma$ /ER $\alpha$ , and 4-fold for 14-3-3 $\sigma$ /USP8 (Figure 3D and Table 1).

**Table 1. Tethering and Stabilization of 14-3-3 $\sigma$ /Clients by Compound 1**

peptide	MSDR (250 $\mu$ M BME)	FADR (50 $\mu$ M BME)	protein titrations (50 $\mu$ M BME)		
	DR <sub>50</sub> ( $\mu$ M)	EC <sub>50</sub> ( $\mu$ M)	K <sub>D_app</sub>	K <sub>D_DMSO</sub>	fold stab.
CRAF	0.007	0.922	106 nM	8.5 $\mu$ M	81
ER $\alpha$	18.1	1.31	21 nM	360 nM	19
USP8	0.024	3.38	1.1 $\mu$ M	4.5 $\mu$ M	4
SOS1	>2 mM	>2 mM	N/A	N/A	N/A
FOXO1	>2 mM	>2 mM	N/A	N/A	N/A
<i>apo</i>	>2 mM	>2 mM	N/A	N/A	N/A

Crystal structures for compound **1** were obtained by cocrystallizing with ER $\alpha$ , C-RAF, or USP8 bound to 14-3-3 $\sigma$  (Figure 3E), with clear density for both **1** and the peptides (Figure S4). Comparing the three cocrystal structures, the strongest electron density and ligand occupancy for **1** was observed in the cocrystal structure with ER $\alpha$ . For ER $\alpha$ , the phenyl ring of **1** stacked against the +1 Val with a distance of  $\sim$ 4 Å (Figure 3E). Compound **1** showed an identical binding mode in the presence of C-RAF (Figure 3F), for which the +1 Thr was 3.5 Å from the phenyl ring, while the remainder of the C-RAF peptide wrapped around the fragment. These additional hydrophobic interactions could explain the higher fold stabilization with the C-RAF peptide compared to ER $\alpha$  (Figure 3D,F). Interestingly, **1** shared the binding moiety with N42C-tethered stabilizers that were discovered previously for ER $\alpha$  (Figure 3G).<sup>25</sup> Whereas compound **1**'s chloro-group was not positioned identically, the longer linker of **1** bridged the larger distance from C38 compared to N42C. In the presence of the USP8 peptide, the phenyl ring of **1** was turned, thereby shifting the fragment up and back into the 14-3-3 $\sigma$  pocket (Figure 3E). This conformational change seemed

necessary because the USP8 peptide allowed for less space (Figure 3H). While the +1 Ser of USP8 did not show any specific interaction with **1**, its +4 Ile pushed the fragment toward 14-3-3 $\sigma$ , which was not an ideal position for this fragment as was reflected by the weak electron density and the minimal stabilization for USP8. By contrast, the +4 Val of C-RAF allowed for more space, thereby positioning **1** in a preferred conformation. It is noteworthy that **1** did not stabilize FOXO1 or SOS1 to 14-3-3 $\sigma$ . A crystallographic overlay of **1** with the FOXO1 peptide showed a steric clash with the +1 Trp of FOXO1, explaining its lack of stabilization (Figure S5A). In contrast, the +1 Ala residue of SOS1 would not contact the phenyl ring of **1**, perhaps explaining why no stabilization was observed (Figure S5B).

**FOXO1 Selective Stabilizers.** The FOXO1 peptide showed the highest number of stabilizing hits in our initial screen. For FOXO1, of the 23 initial stabilizers, 21 showed selectivity for the 14-3-3 $\sigma$ /FOXO1 phosphopeptide complex over *apo* 14-3-3 $\sigma$  and the other phosphopeptide clients in the initial screen (Figure 2D). Interestingly, the unique 21 FOXO1-stabilizers had a highly conserved scaffold, with the phenyl ring engaging FOXO1 often decorated with halogens or a triazole moiety (Figure S6). Eight of these compounds were validated in the MSDR (Figure S7). Of the eight compounds, five compounds had enough material to retest and were active in the FADR assays (Figure 4A, Figure S8, and Table S2). The binding affinity of compound **2** to 14-3-3 $\sigma$  was >10,000-fold better in the presence of the FOXO1 phosphopeptide than *apo* 14-3-3 $\sigma$  and all other phosphopeptide clients (DR<sub>50</sub> = 360 nM vs >2 mM; Figure 4B and Table 2). Compounds **3** and **4** had DR<sub>50</sub> values >450-fold and >2,000-fold better, respectively (Table 2 and Figure S7). Compounds **2**, **3**, and **4** showed the greatest fold-stabilization in the protein titrations decreasing 14-3-3 $\sigma$ /FOXO1 K<sub>D</sub> values 5-fold, 4-fold, and 12-fold (Figure 4C, Table 2, and Figure S9). It should be noted that while a high % tethering was observed for the FOXO1 stabilizers, the protein titrations only showed a modest shift in stabilization. This is likely due to the tight binding of the FOXO1 phosphopeptide, with a K<sub>D</sub> value of 50 nM, already close to the limit of detection of this assay.

A cocrystal structure for FOXO1/2/14-3-3 $\sigma$  was obtained, with clear density for both **2** and the FOXO1 peptide (Figure S10A). The phenyl ring of **2** stacked against the front of the FOXO1 peptide consisting of the +1 Trp and the +2 Pro residues (Figure 4D). Strikingly, in the presence of **2**, the Trp of FOXO1 underwent a conformational change to form a hydrogen bond with its NH and the amide carbonyl of **2** (Figure 4E). Moreover, the hydroxyl on the phenyl ring of **2** made a hydrogen bond with the S45 of 14-3-3 $\sigma$ , explaining the benefit of a hydrogen donor or, potentially, acceptor at that position. Compound **3** was also cocrystallized with FOXO1 (Figure S10B), showing a highly similar binding mode, but a lack of the hydrogen bonding with S45 of 14-3-3 $\sigma$  (Figure S10C). An overlay of **2** with the other peptides revealed that **2** could not reach the smaller +1 residues in the other client peptides or that the peptides sterically clashed (Figure S11), potentially explaining its selectivity for FOXO1 over the other peptides. Previous work discovered imine-based stabilizers for the 14-3-3/Pin-1 complex which, similar to FOXO1, has a +1 Trp.<sup>42</sup> In that work, the Trp engaged in  $\pi$ – $\pi$  stacking interactions with an aromatic ring of the stabilizers. By contrast, the +2 Pro of FOXO1 locked the conformation of the +1 Trp and thereby prevented such a  $\pi$ – $\pi$  stacking interaction

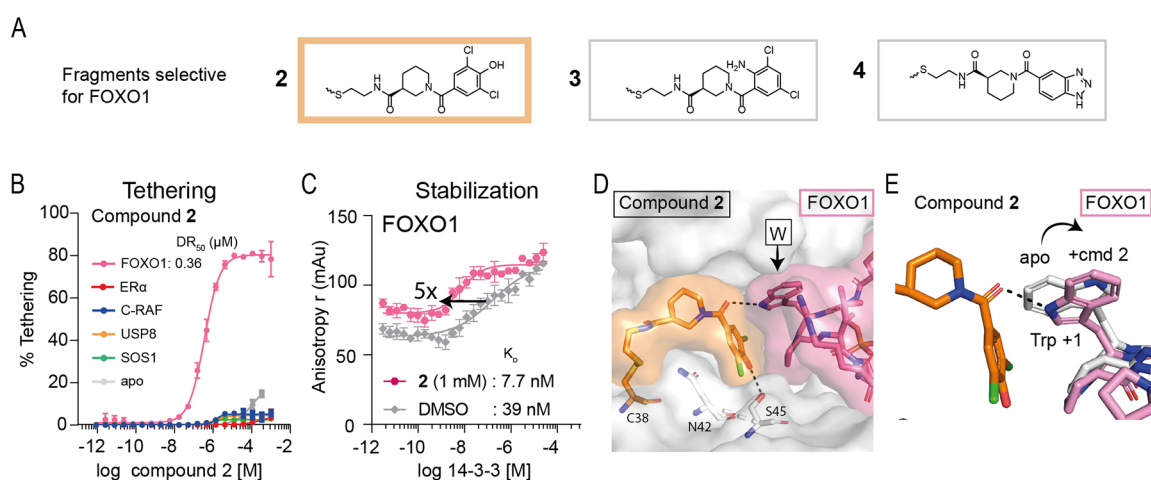


**Figure 4.** Overview of selective stabilizers for FOXO1. (A) Chemical structures of highlighted FOXO1 selective stabilizers 2–4. (B) MSDR curves for 2 showing the percentage of fragment/protein conjugate formation with 14-3-3 $\sigma$  *apo*, or in the presence of ER $\alpha$ , FOXO1, C-RAF, USP8, or SOS1 peptide. (C) 14-3-3 $\sigma$  titrations to fluorescein-labeled FOXO1 in the presence of DMSO or 2 (1 mM), reporting a 5-fold increase in 14-3-3 $\sigma$ /FOXO1 binding. (D) Crystal structure of 2 (orange) bound to 14-3-3 $\sigma$  (white) C38 in complex with FOXO1 phosphopeptide (pink). (E) Overlay of FOXO1 peptide in the *apo*-structure (white) with the FOXO peptide (pink) in the presence of 2 (orange).

**Table 2. Properties of Selective FOXO1 stabilizers**

Cmpnd	MSDR (250 $\mu$ M BME)	FADR (50 $\mu$ M BME)	protein titrations (50 $\mu$ M BME)		
	DR <sub>50</sub> ( $\mu$ M)	EC <sub>50</sub> ( $\mu$ M)	K <sub>D, app</sub> (nM)	K <sub>D, DMSO</sub> <sup>a</sup> (nM)	fold stab.
2	0.36	5.10	7.7	39	5
3	2.2	N/A	10.6	42	4
4	143	N/A	9.7	111	12

<sup>a</sup>K<sub>D</sub> for peptide is accurate within 3-fold range. These values are shown on the same plate as protein titrations with compound.

with 2, while the +2 Arg of Pin-1 allowed  $\pi$ - $\pi$  stacking to take place. Thus, while the compound 2/3 scaffold emphasized the chemical moieties necessary for stabilizing FOXO1, crystal structures also expose a lack of flexibility of the FOXO1 peptide.

**C-RAF Selective Stabilizers.** Following FOXO1, C-RAF had the highest number of stabilizers. Of the 21 initial C-RAF stabilizers, 16 compounds showed selectivity for the 14-3-3 $\sigma$ /C-RAF phosphopeptide complex over *apo* 14-3-3 $\sigma$  and the other phosphopeptide clients in the primary screen (Figure 2D). Eleven compounds showed a similar scaffold which was remarkably analogous to the conserved scaffold for the FOXO1 stabilizers (Figure S12). However, the linker element of these compounds was often longer in the case of C-RAF, and the phenyl ring was decorated with large cyclic groups, while for FOXO1 only smaller halogen groups were tolerated. This is likely due to the smaller +1 residue of C-RAF (Thr for C-RAF, Trp for FOXO1), thereby leaving more space for the compound. Furthermore, two C-RAF stabilizers were shared with ER $\alpha$ , both of which have a similar size in the +1 residue (Val for ER $\alpha$ , Thr for C-RAF). Nine of the 16 selective compounds were validated for potency and selectivity in the MSDR (Figure S13). Four of the nine compounds (compounds 5–8; Figure 5A) showed activity in FADR (Figure S14 and Table S3) and stabilization in the protein titrations (Table 3 and Figure S15).

Compounds 5 and 6 were the most effective stabilizers. Compound 5 had a DR<sub>50</sub> value >3,000-fold lower in the presence of the C-RAF peptide compared to 14-3-3 $\sigma$  alone

(Figure 5B) and showed a 246-fold stabilization of the 14-3-3 $\sigma$ /C-RAF phosphopeptide complex (K<sub>D</sub> = 23  $\mu$ M to 92 nM; Figure 5C). Compound 6 had a DR<sub>50</sub> value 230-fold lower in the presence of C-RAF compared to *apo* 14-3-3 $\sigma$  and a 426-fold stabilization of the 14-3-3 $\sigma$ /C-RAF complex (Table 3, Figures S13 and S15).

The crystal structure of 5 with C-RAF and 14-3-3 $\sigma$  revealed a contact between the naphthalene ring of 5 and the +1 Thr residue of C-RAF. The (*R*)-methyl group of 5 also seems important for hydrophobic interactions with the methyl of the +1 Thr residue of C-RAF, at a distance of 3.8 Å (Figure 5D, Figure S16A). An overlay of the C-RAF peptide in the presence of 5 with the *apo* C-RAF peptide showed no change in conformation of the +1 Thr residue. In contrast, the +4 Val residue of the C-RAF peptide changed conformation to make space for 5 (Figure 5E).

We also crystallized compound 7 as a representative of the other structural class of the selective C-RAF stabilizers (Figure S16B). Compound 7 had a DR<sub>50</sub> value >228-fold lower in the presence of the C-RAF peptide than *apo* 14-3-3 $\sigma$  (Figure 5F) and was less selective for C-RAF compared to 5 in the MSDR (Figure S13). However, compound 7 showed no stabilization of any of the peptides other than C-RAF in the FADR (Figure S14C), reflecting the selectivity shown in the primary screen. The weaker 14-3-3 $\sigma$  binding of 7 (12.2  $\mu$ M DR<sub>50</sub>) was reflected in a somewhat lower stabilization of the 14-3-3 $\sigma$ /C-RAF complex compared to the other chemotype of 5 and 6 (77-fold vs 246- and 426-fold, respectively; Figure 5G, Figure S15). Cocrystallization of 7 with C-RAF and 14-3-3 $\sigma$  revealed a novel orientation of its phenyl ring toward the roof of 14-3-3 $\sigma$ , positioning its trifluoromethyl group above the C-RAF peptide (Figure 5H). While the conformations of 5 and 7 were quite different, an overlay of the two structures showed that the trifluoromethyl group of 7 occupied the same cavity as the naphthalene ring of 5 (Figure S16C). Furthermore, an overlay of the C-RAF peptide in the presence of 7 with the *apo* C-RAF peptide revealed a conformational change of the +4 Val of C-RAF, which stacked against the compound, pushing it toward 14-3-3 $\sigma$ . Additionally, a water-mediated hydrogen bond was formed between 7 and the backbone of the C-RAF peptide

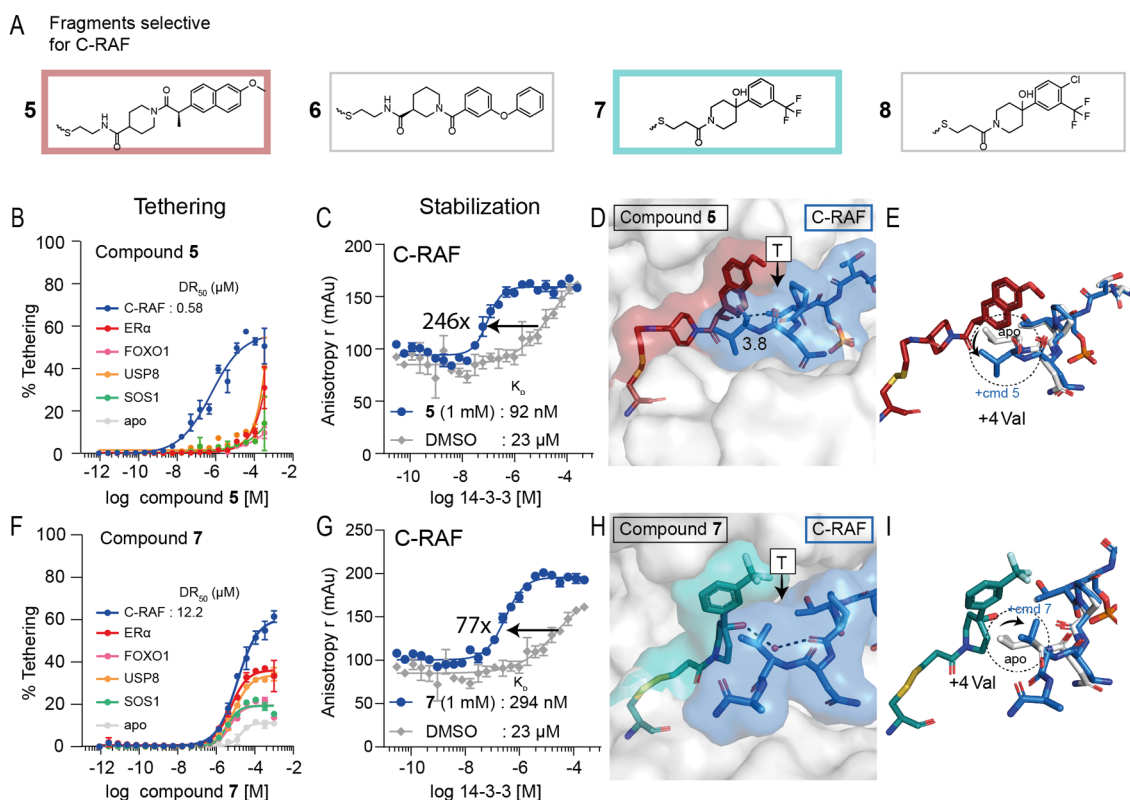


**Figure 5.** Overview of selective stabilizers for C-RAF. (A) Chemical structures of highlighted C-RAF selective stabilizers 5–8. (B) MSDR curves for 5 showing percentage of fragment/protein conjugate formation with 14-3-3 $\sigma$  *apo*, or in the presence of ER $\alpha$ , FOXO1, C-RAF, USP8, or SOS1 peptide. (C) 14-3-3 $\sigma$  titration to fluorescein-labeled C-RAF in the presence of DMSO or 5 (1 mM), reporting a 246-fold increase of 14-3-3 $\sigma$ /C-RAF binding. (D) Crystal structure of 5 (red) bound to 14-3-3 $\sigma$  (white) in complex with C-RAF phosphopeptide (blue). (E) Overlay of C-RAF peptide in the *apo*-structure (white) with the C-RAF peptide (blue) in the presence of 5 (red). (F) MSDR curves for 7 showing percentage of fragment/protein conjugate formation with 14-3-3 $\sigma$  *apo*, or in the presence of ER $\alpha$ , FOXO1, C-RAF, USP8, or SOS1 peptide. (G) 14-3-3 $\sigma$  titration to fluorescein-labeled C-RAF in the presence of DMSO or 7 (1 mM), reporting a 77-fold increase of 14-3-3 $\sigma$ /C-RAF binding. (H) Crystal structure of 7 (teal) bound to 14-3-3 $\sigma$  (white) in complex with C-RAF phosphopeptide (blue). (I) Overlay of C-RAF peptide in the *apo*-structure (white) with the C-RAF peptide (blue) in the presence of 7 (teal).

**Table 3. Properties of Selective C-RAF Stabilizers**

Cmpnd	MSDR (250 $\mu$ M BME)	FADR (50 $\mu$ M BME)	protein titrations (50 $\mu$ M BME)		
	DR <sub>50</sub> ( $\mu$ M)	EC <sub>50</sub> ( $\mu$ M)	$K_{D, app}$ (nM)	$K_{D, DMSO}^{a}$ ( $\mu$ M)	fold stab.
5	0.58	0.22	92	23	246
6	8.78	1.33	100	42	426
7	12.2	3.18	294	23	77
8	3.71	13.5	207	23	110

<sup>a</sup> $K_D$  for peptide is accurate within a 3-fold range. These values are shown on the same plate as protein titrations with compound.

(Figure S1). The lower specificity for C-RAF of 7 in the MSDR could be due to its small size, leaving room for alternative +1 residues to have a cooperative effect on 14-3-3 $\sigma$  engagement. Stabilizer 8 had an almost identical structure to 7, differing only in a chloro-group in the para-position of the phenyl ring, and showed binding modes similar to 7 in its structure with C-RAF (Figure S16D,E).

Next to these C-RAF selective stabilizers, the nonselective stabilizer compound 1 also showed a large fold-stabilization toward the C-RAF peptide (Figure 3). A crystallographic overlay of these three scaffolds revealed remarkable differences in conformation of the C-RAF/compound interactions (Figure S16F). These changes highlight the flexibility of the C-RAF

peptide, perhaps leading to its facility for stabilization, especially in the case of the stabilizers' phenyl ring, which can occupy a wide range of positions and conformations in combination with the C-RAF client phosphopeptide.

## CONCLUSIONS

Systematic methods to discover small-molecule stabilizers of PPIs would enable chemical biologists to probe challenging biological systems with potency and precision. By trapping proteins in complexes, stabilization can target proteins with intrinsically disordered regions and allow manipulation of a specific PPI from among related hub protein complexes within a network. Disulfide tethering, a powerful FBDD technique, is readily tunable to a specific site on a protein of interest, amenable to HTS, and provides a direct quantitative measurement of fragment binding.

Here, we explored the scope of the disulfide tethering technology using the hub protein 14-3-3 $\sigma$  and 5 biologically and structurally diverse phosphopeptides derived from the 14-3-3 client proteins ER $\alpha$ , FOXO1, C-RAF, USP8, and SOS1. Of the 1600 fragments in the disulfide library, 62 showed activity as stabilizers for one or more phosphopeptides and were assessed by MSDR. 36 of the 62 compounds were taken forward into the FADR assays to determine stabilization of a 14-3-3 client phosphopeptide. Finally, eight compounds



showed cooperativity with the 14-3-3 $\sigma$ /phosphopeptide complex via 14-3-3 $\sigma$  protein titrations, and six were structurally characterized for their contacts with 14-3-3 $\sigma$  and the client phosphopeptide via X-ray crystallography (Figure S17A). Thus, the disulfide tethering strategy systematically discovered stabilizers for a range of peptide sequences, conformations, and affinities.

Of the 5 peptide targets selected, we discovered stabilizers for four clients, two of which also had selective stabilizers. Fragments increased the binding affinity of the 14-3-3 $\sigma$ /phosphopeptide complex as much as 430-fold in the case of **6** and 250-fold for our best structurally characterized hit, **5**. Selective stabilizers distinguished between phosphopeptide clients due to the unique composite binding surface created by the phosphopeptide/14-3-3 $\sigma$  interface (Figures 4 and 5). The nonselective stabilizers also showed varying degrees of efficacy in stabilizing different clients. Compound **1** facilitated a greater than 80-fold shift in affinity for C-RAF, a 19-fold shift for ER $\alpha$ , a more modest 4-fold shift for USP8, but had no effect on SOS1 and FOXO1 (Figure 3).

The individual phosphopeptide binding motifs and C-terminal residues following the phosphorylation site created a distinct environment around the 14-3-3 $\sigma$  C38 fragment binding pocket, dictating what chemical moieties effectively facilitated cooperativity between 14-3-3 $\sigma$ , the phosphopeptide client, and the fragments. The stabilizers for FOXO1 had a highly conserved scaffold, consistent with the rigidity of this peptide (Figure S17B). In contrast, the stabilizers of C-RAF were larger and showed more chemical diversity in their scaffold, emphasizing the flexibility of the C-RAF peptide. The short ER $\alpha$  peptide resulted in limited selectivity, sharing many stabilizers with C-RAF. Lastly, USP8 and SOS1 were the hardest to target, likely due to the proximity of the peptide C-terminus to C38 of 14-3-3 $\sigma$ , which was also reflected in the small scaffold of the discovered stabilizers from the primary screen (Figure S17B). Alternative cysteine tethering mutations could sample different subpockets to stabilize peptides which occupy more of the 14-3-3 binding groove. Taken together, the intrinsic diversity of the 14-3-3/phosphopeptide composite binding interface allowed for selectivity and precision when targeting a specific 14-3-3/client PPI.

The stabilizing fragments we discovered can be further optimized for chemical biology and therapeutics applications. For instance, 14-3-3/FOXO1 stabilization could inhibit FOXO1-fusion proteins in rare cancers and correct metabolism in diabetes.<sup>43,44</sup> Additionally, 14-3-3-mediated inhibition of C-RAF is strongly implicated in RAS-mediated cancers and in the developmental disorder Noonan's syndrome, where mutations in C-RAF and other proteins in the pathway lead to slight upregulation of MAP kinase signaling.<sup>32,39</sup>

While the focus of the screen was the discovery of fragment stabilizers, the screen also identified selective inhibitors, nonselective inhibitors, and neutral compounds for each client peptide and 14-3-3 (Figure S18). Therefore, disulfide tethering is a versatile tool that can be expanded to meet a wide range of conditions and results in hits that disrupt or stabilize PPIs. 14-3-3 provides an exciting proof of concept due to its large roster of clients, involvement in many biological processes, therapeutic potential, and extensive structural data, but the applicability of FBDD reaches beyond targeting a singular protein. It is due to this ease of access and applicability that disulfide tethering lends itself to the discovery of biological probes for PPIs and novel therapeutics for previously

inaccessible biological challenges and diseases related to intrinsically disordered proteins.

## ■ ASSOCIATED CONTENT

### Supporting Information

The Supporting Information is available free of charge at <https://pubs.acs.org/doi/10.1021/acscentsci.2c01449>.

Experimental methods, tethering and stabilization data of primary screen (Tables S1–S5), XRD data collection and refinement statistics (Tables S6 and S7), MSDR and FADR binding curves of the validation approach (Figures S2, S3, S7, S8, S9, S13–S15), X-ray density and crystallographic overlay of disulfide fragments (Figures S4, S5, S10, S11, S16), chemical structures and information of discovered fragments of the primary screen (Figures S6, S12, S17, S18) (PDF)

## ■ AUTHOR INFORMATION

### Corresponding Authors

**Michelle R. Arkin** – Department of Pharmaceutical Chemistry and Small Molecule Discovery Center (SMDC), University of California, San Francisco 94143, United States;  
orcid.org/0000-0002-9366-6770;  
Email: [michelle.arkin@ucsf.edu](mailto:michelle.arkin@ucsf.edu)

**Christian Ottmann** – Laboratory of Chemical Biology, Department of Biomedical Engineering and Institute for Complex Molecular Systems (ICMS), Eindhoven University of Technology, 5600 MB Eindhoven, The Netherlands;  
orcid.org/0000-0001-7315-0315; Email: [c.ottmann@tue.nl](mailto:c.ottmann@tue.nl)

**Luc Brunsveld** – Laboratory of Chemical Biology, Department of Biomedical Engineering and Institute for Complex Molecular Systems (ICMS), Eindhoven University of Technology, 5600 MB Eindhoven, The Netherlands;  
orcid.org/0000-0001-5675-511X; Email: [l.brunsveld@tue.nl](mailto:l.brunsveld@tue.nl)

### Authors

**Dyana N. Kenanova** – Department of Pharmaceutical Chemistry and Small Molecule Discovery Center (SMDC), University of California, San Francisco 94143, United States

**Emira J. Visser** – Laboratory of Chemical Biology, Department of Biomedical Engineering and Institute for Complex Molecular Systems (ICMS), Eindhoven University of Technology, 5600 MB Eindhoven, The Netherlands

**Johanna M. Virta** – Department of Pharmaceutical Chemistry and Small Molecule Discovery Center (SMDC), University of California, San Francisco 94143, United States

**Eline Sijbesma** – Laboratory of Chemical Biology, Department of Biomedical Engineering and Institute for Complex Molecular Systems (ICMS), Eindhoven University of Technology, 5600 MB Eindhoven, The Netherlands

**Federica Centorrino** – Laboratory of Chemical Biology, Department of Biomedical Engineering and Institute for Complex Molecular Systems (ICMS), Eindhoven University of Technology, 5600 MB Eindhoven, The Netherlands

**Holly R. Vickery** – Department of Pharmaceutical Chemistry and Small Molecule Discovery Center (SMDC), University of California, San Francisco 94143, United States

**Mengqi Zhong** – Department of Pharmaceutical Chemistry and Small Molecule Discovery Center (SMDC), University of

California, San Francisco 94143, United States;

[orcid.org/0000-0003-0525-6999](https://orcid.org/0000-0003-0525-6999)

R. Jeffrey Neitz – Department of Pharmaceutical Chemistry and Small Molecule Discovery Center (SMDC), University of California, San Francisco 94143, United States

Complete contact information is available at:

<https://pubs.acs.org/10.1021/acscentsci.2c01449>

### Author Contributions

<sup>†</sup>D.N.K. and E.J.V. contributed equally to this work. The manuscript was written through contributions of all authors. All authors have given approval to the final version of the manuscript.

### Funding

This research was funded by the ONO Pharma Foundation Breakthrough Science Initiative Award (M.R.A.), the National Institutes of Health grant GM14796, Netherlands Organization for Scientific Research (NWO) through the Gravity program 024.001.035, and ECHO grant 711.018.003.

### Notes

The authors declare the following competing financial interest(s): M.R.A., L.B. and C.O. are founders of Ambagon Therapeutics. M.R.A. is a director, L.B. is a member of Ambagon's scientific advisory board, C.O., E.S are employees of Ambagon.

### ACKNOWLEDGMENTS

We thank the Renslo laboratory as well as Paul Burroughs and Joshua Ramos for the synthesis of the disulfide library; we also thank Julia Davies, Grace Pohan, and Amanda Paulson for the automated MS data processing infrastructure in the SMDC and compound data clustering. We thank Markella Konstantinidou and Priya Jaishankar for support with synthetic strategy and John Morrow for contributions in the initial stage of the 14-3-3 tethering project. We acknowledge DESY (Hamburg, Germany), a member of the Helmholtz Association HGF, for the provision of experimental facilities. Parts of this research were carried out at PETRA III, and we would like to thank Johanna Hakanpää and Anja Burkhardt for assistance in using beam P11. Beamtime was allocated for proposals 11011126, 11012787, and 11006723. Further, we thank Diamond Light Source for beamtime (proposal mx19800-27), and the staff of beamline I03 for assistance with crystal testing and data collection.

### REFERENCES

- (1) Garlick, J. M.; Mapp, A. K. Selective Modulation of Dynamic Protein Complexes. *Cell Chem. Biol.* **2020**, *27* (8), 986–997.
- (2) Ivanov, A. A.; Revennaugh, B.; Rusnak, L.; Gonzalez-Pecchi, V.; Mo, X.; Johns, M. A.; Du, Y.; Cooper, L. A. D.; Moreno, C. S.; Khuri, F. R.; Fu, H. The OncoPPI Portal: An Integrative Resource to Explore and Prioritize Protein-Protein Interactions for Cancer Target Discovery. *Bioinforma. Oxf. Engl.* **2018**, *34* (7), 1183–1191.
- (3) Kim, M.; Park, J.; Bouhaddou, M.; Kim, K.; Rojic, A.; Modak, M.; Soucheray, M.; McGregor, M. J.; O'Leary, P.; Wolf, D.; Stevenson, E.; Foo, T. K.; Mitchell, D.; Herrington, K. A.; Munoz, D. P.; Tutuncuoglu, B.; Chen, K.-H.; Zheng, F.; Kreisberg, J. F.; Diolaiti, M. E.; Gordan, J. D.; Coppe, J.-P.; Swaney, D. L.; Xia, B.; van 't Veer, L.; Ashworth, A.; Ideker, T.; Krogan, N. J. A Protein Interaction Landscape of Breast Cancer. *Science* **2021**, *374* (6563), abf3066.
- (4) Wright, M. T.; Plate, L. Revealing Functional Insights into ER Proteostasis through Proteomics and Interactomics. *Exp. Cell Res.* **2021**, *399* (1), 112417.

- (5) Hu, G.; Wu, Z.; Uversky, V. N.; Kurgan, L. Functional Analysis of Human Hub Proteins and Their Interactors Involved in the Intrinsic Disorder-Enriched Interactions. *Int. J. Mol. Sci.* **2017**, *18* (12), No. E2761.

- (6) Arkin, M. R.; Tang, Y.; Wells, J. A. Small-Molecule Inhibitors of Protein-Protein Interactions: Progressing toward the Reality. *Chem. Biol.* **2014**, *21* (9), 1102–1114.

- (7) Celis, S.; Hobor, F.; James, T.; Bartlett, G. J.; Ibarra, A. A.; Shoemark, D. K.; Hegedüs, Z.; Hetherington, K.; Woolfson, D. N.; Sessions, R. B.; Edwards, T. A.; Andrews, D. M.; Nelson, A.; Wilson, A. J. Query-Guided Protein-Protein Interaction Inhibitor Discovery. *Chem. Sci.* **2021**, *12* (13), 4753–4762.

- (8) Linhares, B. M.; Grembecka, J.; Cierpicki, T. Targeting Epigenetic Protein-Protein Interactions with Small-Molecule Inhibitors. *Future Med. Chem.* **2020**, *12* (14), 1305–1326.

- (9) Modell, A. E.; Blosser, S. L.; Arora, P. S. Systematic Targeting of Protein-Protein Interactions. *Trends Pharmacol. Sci.* **2016**, *37* (8), 702–713.

- (10) Zhong, M.; Lee, G. M.; Sijbesma, E.; Ottmann, C.; Arkin, M. R. Modulating Protein-Protein Interaction Networks in Protein Homeostasis. *Curr. Opin. Chem. Biol.* **2019**, *50*, 55–65.

- (11) Andrei, S. A.; Sijbesma, E.; Hann, M.; Davis, J.; O'Mahony, G.; Perry, M. W. D.; Karawajczyk, A.; Eickhoff, J.; Brunsveld, L.; Doveston, R. G.; Milroy, L.-G.; Ottmann, C. Stabilization of Protein-Protein Interactions in Drug Discovery. *Expert Opin. Drug Discovery* **2017**, *12* (9), 925–940.

- (12) Tang, C.; Mo, X.; Niu, Q.; Wahafu, A.; Yang, X.; Qui, M.; Ivanov, A. A.; Du, Y.; Fu, H. Hypomorph Mutation-Directed Small-Molecule Protein-Protein Interaction Inducers to Restore Mutant SMAD4-Suppressed TGF- $\beta$  Signaling. *Cell Chem. Biol.* **2021**, *28* (5), 636–647.

- (13) Stevers, L. M.; Sijbesma, E.; Botta, M.; MacKintosh, C.; Obsil, T.; Landrieu, I.; Cau, Y.; Wilson, A. J.; Karawajczyk, A.; Eickhoff, J.; Davis, J.; Hann, M.; O'Mahony, G.; Doveston, R. G.; Brunsveld, L.; Ottmann, C. Modulators of 14-3-3 Protein-Protein Interactions. *J. Med. Chem.* **2018**, *61* (9), 3755–3778.

- (14) De Vries-van Leeuwen, I. J.; da Costa Pereira, D.; Flach, K. D.; Piersma, S. R.; Haase, C.; Bier, D.; Yalcin, Z.; Michalides, R.; Feenstra, K. A.; Jiménez, C. R.; de Greef, T. F. A.; Brunsveld, L.; Ottmann, C.; Zwart, W.; de Boer, A. H. Interaction of 14–3-3 Proteins with the Estrogen Receptor Alpha F Domain Provides a Drug Target Interface. *Proc. Natl. Acad. Sci. U. S. A.* **2013**, *110* (22), 8894–8899.

- (15) Mayor-Ruiz, C.; Bauer, S.; Brand, M.; Kozicka, Z.; Siklos, M.; Imrichova, H.; Kaltheuner, I. H.; Hahn, E.; Seiler, K.; Koren, A.; Petzold, G.; Fellner, M.; Bock, C.; Müller, A. C.; Zuber, J.; Geyer, M.; Thomä, N. H.; Kubicek, S.; Winter, G. E. Rational Discovery of Molecular Glue Degradors via Scalable Chemical Profiling. *Nat. Chem. Biol.* **2020**, *16* (11), 1199–1207.

- (16) Chamberlain, P. P.; Cathers, B. E. Cereblon Modulators: Low Molecular Weight Inducers of Protein Degradation. *Drug Discovery Today Technol.* **2019**, *31*, 29–34.

- (17) Slabicki, M.; Kozicka, Z.; Petzold, G.; Li, Y.-D.; Manojkumar, M.; Bunker, R. D.; Donovan, K. A.; Sievers, Q. L.; Koeppl, J.; Suchyta, D.; Sperling, A. S.; Fink, E. C.; Gasser, J. A.; Wang, L. R.; Corsello, S. M.; Sellar, R. S.; Jan, M.; Gillingham, D.; Scholl, C.; Fröhling, S.; Golub, T. R.; Fischer, E. S.; Thomä, N. H.; Ebert, B. L. The CDK Inhibitor CR8 Acts as a Molecular Glue Degradator That Depletes Cyclin K. *Nature* **2020**, *585* (7824), 293–297.

- (18) Hartman, A. M.; Elgaher, W. A. M.; Hertrich, N.; Andrei, S. A.; Ottmann, C.; Hirsch, A. K. H. Discovery of Small-Molecule Stabilizers of 14–3-3 Protein-Protein Interactions via Dynamic Combinatorial Chemistry. *ACS Med. Chem. Lett.* **2020**, *11* (5), 1041–1046.

- (19) Pfaff, S. J.; Chimenti, M. S.; Kelly, M. J. S.; Arkin, M. R. Biophysical Methods for Identifying Fragment-Based Inhibitors of Protein-Protein Interactions. In *Protein-Protein Interactions: Methods and Applications*; Meyerkord, C. L., Fu, H., Eds.; Methods in Molecular Biology; Springer: New York, NY, 2015; pp 587–613. DOI: 10.1007/978-1-4939-2425-7\_39.

- (20) Erlanson, D. A.; Arndt, J. W.; Cancelli, M. T.; Cao, K.; Elling, R. A.; English, N.; Friedman, J.; Hansen, S. K.; Hession, C.; Joseph, L.; Kumaravel, G.; Lee, W.-C.; Lind, K. E.; McDowell, R. S.; Miatkowski, K.; Nguyen, C.; Nguyen, T. B.; Park, S.; Pathan, N.; Penny, D. M.; Romanowski, M. J.; Scott, D.; Silvian, L.; Simmons, R. L.; Tangonan, B. T.; Yang, W.; Sun, L. Discovery of a Potent and Highly Selective PDK1 Inhibitor via Fragment-Based Drug Discovery. *Bioorg. Med. Chem. Lett.* **2011**, *21* (10), 3078–3083.
- (21) Hallenbeck, K. K.; Davies, J. L.; Merron, C.; Ogden, P.; Sijbesma, E.; Ottmann, C.; Renslo, A. R.; Wilson, C.; Arkin, M. R. A Liquid Chromatography/Mass Spectrometry Method for Screening Disulfide Tethering Fragments. *SLAS Discovery Adv. Life Sci. R D* **2018**, *23* (2), 183–192.
- (22) Raimundo, B. C.; Oslob, J. D.; Braisted, A. C.; Hyde, J.; McDowell, R. S.; Randal, M.; Waal, N. D.; Wilkinson, J.; Yu, C. H.; Arkin, M. R. Integrating Fragment Assembly and Biophysical Methods in the Chemical Advancement of Small-Molecule Antagonists of IL-2: An Approach for Inhibiting Protein-Protein Interactions. *J. Med. Chem.* **2004**, *47* (12), 3111–3130.
- (23) Lodge, J. M.; Rettenmaier, T. J.; Wells, J. A.; Pomerantz, W. C.; Mapp, A. K. FP Tethering: A Screening Technique to Rapidly Identify Compounds That Disrupt Protein-Protein Interactions. *MedChemComm* **2014**, *5*, 370–375.
- (24) Sadowsky, J. D.; Burlingame, M. A.; Wolan, D. W.; McClendon, C. L.; Jacobson, M. P.; Wells, J. A. Turning a Protein Kinase on or off from a Single Allosteric Site via Disulfide Trapping. *Proc. Natl. Acad. Sci. U. S. A.* **2011**, *108* (15), 6056–6061.
- (25) Sijbesma, E.; Hallenbeck, K. K.; Leysen, S.; de Vink, P. J.; Skóra, L.; Jahnke, W.; Brunsfeld, L.; Arkin, M. R.; Ottmann, C. Site-Directed Fragment-Based Screening for the Discovery of Protein-Protein Interaction Stabilizers. *J. Am. Chem. Soc.* **2019**, *141* (8), 3524–3531.
- (26) Burlingame, M. A.; Tom, C. T. M. B.; Renslo, A. R. Simple One-Pot Synthesis of Disulfide Fragments for Use in Disulfide-Exchange Screening. *ACS Comb. Sci.* **2011**, *13* (3), 205–208.
- (27) Morrison, D. K. The 14–3-3 Proteins: Integrators of Diverse Signaling Cues That Impact Cell Fate and Cancer Development. *Trends Cell Biol.* **2009**, *19* (1), 16–23.
- (28) Obsilova, V.; Obsil, T. The 14-3-3 Proteins as Important Allosteric Regulators of Protein Kinases. *Int. J. Mol. Sci.* **2020**, *21* (22), No. E8824.
- (29) Aghazadeh, Y.; Papadopoulos, V. The Role of the 14–3-3 Protein Family in Health, Disease, and Drug Development. *Drug Discovery Today* **2016**, *21* (2), 278–287.
- (30) Gardino, A. K.; Smerdon, S. J.; Yaffe, M. B. Structural Determinants of 14–3-3 Binding Specificities and Regulation of Subcellular Localization of 14–3-3-Ligand Complexes: A Comparison of the X-Ray Crystal Structures of All Human 14–3-3 Isoforms. *Semin. Cancer Biol.* **2006**, *16* (3), 173–182.
- (31) Zhao, J.; Meyerkord, C. L.; Du, Y.; Khuri, F. R.; Fu, H. 14–3-3 Proteins as Potential Therapeutic Targets. *Semin. Cell Dev. Biol.* **2011**, *22* (7), 705–712.
- (32) Molzan, M.; Kasper, S.; Röglin, L.; Skwarczynska, M.; Sassa, T.; Inoue, T.; Breitenbuecher, F.; Ohkanda, J.; Kato, N.; Schuler, M.; Ottmann, C. Stabilization of Physical RAF/14–3-3 Interaction by Cotylenin A as Treatment Strategy for RAS Mutant Cancers. *ACS Chem. Biol.* **2013**, *8* (9), 1869–1875.
- (33) RCSB PDB: Homepage. <https://www.rcsb.org/> (accessed 2022-06-21).
- (34) Liau, N. P. D.; Wendorff, T. J.; Quinn, J. G.; Steffek, M.; Phung, W.; Liu, P.; Tang, J.; Irudayanathan, F. J.; Izadi, S.; Shaw, A. S.; Malek, S.; Hymowitz, S. G.; Sudhamsu, J. Negative Regulation of RAF Kinase Activity by ATP Is Overcome by 14–3-3-Induced Dimerization. *Nat. Struct. Mol. Biol.* **2020**, *27* (2), 134–141.
- (35) Ballone, A.; Lau, R. A.; Zweipfenning, F. P. A.; Ottmann, C. A New Soaking Procedure for X-Ray Crystallographic Structural Determination of Protein-Peptide Complexes. *Acta Crystallogr. Sect. F Struct. Biol. Commun.* **2020**, *76* (10), 501–507.
- (36) Saha, M.; Carriere, A.; Cheerathodi, M.; Zhang, X.; Lavoie, G.; Rush, J.; Roux, P. P.; Ballif, B. A. RSK Phosphorylates SOS1 Creating 14–3-3-Docking Sites and Negatively Regulating MAPK Activation. *Biochem. J.* **2012**, *447* (1), 159–166.
- (37) Saline, M.; Badertscher, L.; Wolter, M.; Lau, R.; Gunnarsson, A.; Jacso, T.; Norris, T.; Ottmann, C.; Snijder, A. AMPK and AKT Protein Kinases Hierarchically Phosphorylate the N-Terminus of the FOXO1 Transcription Factor, Modulating Interactions with 14–3-3 Proteins. *J. Biol. Chem.* **2019**, *294* (35), 13106–13116.
- (38) Centorrino, F.; Ballone, A.; Wolter, M.; Ottmann, C. Biophysical and Structural Insight into the USP8/14–3-3 Interaction. *FEBS Lett.* **2018**, *592* (7), 1211–1220.
- (39) Molzan, M.; Schumacher, B.; Ottmann, C.; Baljuls, A.; Polzien, L.; Weyand, M.; Thiel, P.; Rose, R.; Rose, M.; Kuhenne, P.; Kaiser, M.; Rapp, U. R.; Kuhlmann, J.; Ottmann, C. Impaired Binding of 14–3-3 to C-RAF in Noonan Syndrome Suggests New Approaches in Diseases with Increased Ras Signaling. *Mol. Cell. Biol.* **2010**, *30* (19), 4698–4711.
- (40) Falcicchio, M.; Ward, J. A.; Chothia, S. Y.; Basran, J.; Mohindra, A.; Macip, S.; Roversi, P.; Doveston, R. G. Cooperative Stabilisation of 14–3-3 $\sigma$  Protein-Protein Interactions via Covalent Protein Modification. *Chem. Sci.* **2021**, *12*, 12985.
- (41) Molzan, M.; Ottmann, C. Synergistic Binding of the Phosphorylated S233- and S259-Binding Sites of C-RAF to One 14–3-3 $\zeta$  Dimer. *J. Mol. Biol.* **2012**, *423* (4), 486–495.
- (42) Cossar, P. J.; Wolter, M.; van Dijk, L.; Valenti, D.; Levy, L. M.; Ottmann, C.; Brunsfeld, L. Reversible Covalent Imine-Tethering for Selective Stabilization of 14–3-3 Hub Protein Interactions. *J. Am. Chem. Soc.* **2021**, *143* (22), 8454–8464.
- (43) Raze, T.; Lapouble, E.; Lacour, B.; Guissou, S.; Defachelles, A.-S.; Gaspar, N.; Delattre, O.; Pierron, G.; Desandes, E. PAX-FOXO1 Fusion Status in Children and Adolescents with Alveolar Rhabdomyosarcoma: Impact on Clinical, Pathological, and Survival Features. *Pediatr. Blood Cancer* **2023**, *70* (4), No. e30228.
- (44) Peng, S.; Li, W.; Hou, N.; Huang, N. A Review of FoxO1-Regulated Metabolic Diseases and Related Drug Discoveries. *Cells* **2020**, *9* (1), 184.